

**Effect of Dynamic Correlation on the Ultrafast Relaxation of
Uracil in the Gas Phase**

Journal:	<i>Faraday Discussions</i>
Manuscript ID	FD-ART-09-2020-000110.R1
Article Type:	Paper
Date Submitted by the Author:	20-Oct-2020
Complete List of Authors:	Chakraborty, Pratip; Temple University, Department of Chemistry Liu, Yusong; Stony Brook University Weinacht, Thomas; Stony Brook University Matsika, Spiridoula; Temple University, Department of Chemistry



Journal Name

Cite this: DOI: 10.1039/xxxxxxxxxx

ARTICLE TYPE

Effect of Dynamic Correlation on the Ultrafast Relaxation of Uracil in the Gas Phase

Pratip Chakraborty,^a Yusong Liu,^b Thomas Weinacht,^b and Spiridoula Matsika^{*a}

Received Date

Accepted Date

DOI: 10.1039/xxxxxxxxxx

www.rsc.org/journalname

The photophysics and photochemistry of DNA/RNA nucleobases have been extensively investigated during the past two decades, both experimentally and theoretically. The ultrafast relaxation of the canonical nucleobases following photoexcitation is of significant interest when it comes to understanding how nature has ensured their photostability. Here we study the excited state dynamics of uracil which is a nucleobase found in RNA. Although theory and experiment have shed a significant light in understanding the photoexcited dynamics of uracil, there are still disagreements in the literature about specific details. In order to examine how the dynamics is influenced by the underlying electronic structure theory, we have performed non-adiabatic excited state dynamics simulations of uracil using on-the-fly trajectory surface hopping methodology on potential energy surfaces calculated at different electronic structure theory levels (CASSCF, MRCIS, XMS-CASPT2, TD-DFT). These simulations reveal that the dynamics are very sensitive to the underlying electronic structure theory, with the multi-reference theory levels that include dynamic correlation predicting that there is no trapping on the absorbing S_2 state, in contrast with predictions from lower level electronic structure results. The dynamics are instead governed by ultrafast decay to the ground state or trapping on the dark S_1 state.

^a Department of Chemistry, Temple University, Philadelphia, Pennsylvania 19122, USA. Tel: +1 215 204 2102; E-mail: smatsika@temple.edu

^b Department of Physics and Astronomy, Stony Brook University, New York 11794, USA.

† Electronic Supplementary Information (ESI) available: Additional details of methodology, analysis, and results. See DOI: 10.1039/b000000x/

1 Introduction

The photophysics and photochemistry of DNA and RNA nucleobases have been investigated extensively in the past two decades, both experimentally and theoretically.^{1–6} Such nucleobases can absorb light in the near UV region leading to creation of excited electronic states. If these nucleobases stay in their excited electronic state for long, they can lead to formation of photoproducts which in turn can develop into carcinogenic photolesions. However, chemical evolution has ensured their photostability *via* ultrafast relaxation through conical intersections (CIs), which is paramount to our survival. After photoexcitation, these bases relax back to the ground state in an ultrafast and non-radiative manner *via* CIs, whereas, the excess energy is redistributed amongst different degrees of freedom in the gas phase and to the surrounding environment in the bulk as heat. Hence, these excited states are short-lived which is evidenced by their low fluorescence quantum yield.^{1,2,6}

Here we investigate the non-adiabatic dynamics of uracil which is a pyrimidine nucleobase found in RNA. A multitude of experimental and theoretical studies have been performed on the photophysics of uracil to understand its ultrafast relaxation back to the ground state.^{1–31} After electronic excitation to the bright S_2 state of uracil, two pathways of relaxation to the ground state have been found to play the most important role. There can be a direct decay to the closed shell ground state from the $\pi\pi^*$ state which goes through two CI seams - the S_2/S_1 and the S_1/S_0 CI, without changing the initial $\pi\pi^*$ state character. The other is an indirect decay where population can get trapped on the dark $n\pi^*$ S_1 state and decay later. Trapping on the S_2 state,^{17,20–22,25} a transfer of population from the dark $n\pi^*$ state to a triplet state,^{28,31} and a deactivation through ring-opening mechanism has also been proposed.²⁵

The development of time-resolved femtosecond (fs) pump-probe spectroscopic techniques has paved the way for investigating the mechanisms underlying photoexcited dynamics in nucleobases. Kang *et al.* reported the first pump-probe experiment on uracil. They used a 267 nm laser to excite the molecules and a near infrared (IR) laser to ionize (*via* multiphoton absorption) and found a mono-exponential decay with a 2.4 picoseconds (ps) lifetime.⁹ Soon after, Ulrich *et al.* measured the time-resolved photoelectron spectrum (TRPES) of uracil using a 250 nm pump and a 200 nm probe and were able to fit three time-constants of <50 fs, 530 fs and 2.4 ps to the photoelectron decay.¹⁰ At the same time, a dark state with a life-time of several nanoseconds has also been found in methylated uracils and thymines by He *et al.* and was explained by trapping in the dark $n\pi^*$ state.^{11,12} Later Canuel *et al.* fitted decay times of 130 fs and 1.1 ps using a 267 nm excitation wavelength and two photon ionization with a 400 nm probe pulse.¹³ Strong-field ionization was also used as probe in conjunction with time-of-flight mass spectrometry (TOFMS) (along with 262 nm pump laser) which produced two decay time-constants: 70-90 fs and 2.2-3.2 ps.^{16,17} TRPES measurements of uracil were carried out more recently by Yu *et al.* using a 260 nm pump and a two-photon 295 nm probe to fit three decay constants

of 170 fs, 2.4 ps and > 1 ns, where the > 1 ns time-constant was attributed to trapping in the triplet states.³⁰ Time-resolved photoion yield measurements were performed again using a 260 nm pump with both strong-field and weak-field ionization (156 nm). The strong-field multiphoton ionization yielded timescales of 65-80 fs and 2.5-3.0 ps, whereas, the 156 nm vacuum UV probe produced timescales of 325-455 fs and 2.0-3.3 ps.²⁹ Ghafur *et al.* also performed time-resolved photoion yield measurements using a laser-based thermal desorption source (while exciting at a 267 nm) to fit time-constants of 200 fs and 3.0 ps.¹⁸ These time-resolved ultrafast spectroscopic studies have demonstrated that the ultrafast relaxation process of uracil is a very complex one with multiple pathways ensuing on different timescales. The timescales generated from the experimental studies are also dependent on the resolution of the experiment. In spite of that, there is a commonality between the experiments that most of them generate two particular time-constants: one shorter time-constant of < 200 fs and another longer one between 2.0-3.3 ps. However, there are different interpretations of the source of these time-constants. Ultrafast studies have also been done in solution, although the solvent may have a pronounced effect on the dynamics as the different lifetimes detected indicate.^{7,8,14,15}

Dynamics simulations to investigate photorelaxation mechanism of uracil have also been performed using both *ab initio* multiple spawning (AIMS)²⁰ and trajectory surface hopping (TSH).²¹⁻²⁸ All of these calculations have been carried out at theory levels such as CASSCF, semiempirical OM2/MRCI and CPMD/BLYP, and most of them obtain a single time-constant which corresponds to the intermediate timescale provided by Ulrich *et al.*¹⁰ Nonetheless, the mechanisms that they propose for deactivation are not the same. Nachtigallová *et al.* have found two time-constants for the decay: one in the intermediate range and the other longer one.²⁵ They have shown the presence of a population trapping on the S_2 state that contributes to the longer time-constant as has been proposed before.²⁰⁻²² In contrast to that, semiempirical OM2/MRCI simulation of Lan *et al.* and CASSCF simulations of Fingerhut *et al.* show very little or no trapping on the S_2 surface.^{23,26,27} Richter *et al.* investigated the involvement of intersystem crossing on the dynamics at the CASSCF level and were able to obtain the shorter and the longer timescales similar to most of the experiments once they fitted the total $S_0 + T_1$ yield of the simulation.²⁸

As discussed before, even though these studies have elucidated a significant amount of detail about the photodynamics of uracil, there are still disagreements in the literature about specific details. The population trapping in the S_1 minimum is universally accepted. However, there has been a great deal of debate on whether population can get trapped on the S_2 state or not. This is because the height of the barrier on the S_2 state calculated using different electronic structure methods varies widely depending on the method. The height of the barrier on S_2 dictates how the dynamics play out. The calculated barrier on S_2 is higher when complete active space self-consistent field (CASSCF) method is employed compared to when higher level electronic structure methods such as multi-reference configuration interaction (MRCI), multi-state complete active space second order pertur-

bation theory (MS-CASPT2) and equation-of-motion coupled cluster method with singles and doubles (EOM-CCSD) are used.^{17,19,32,33} At the CASSCF level, differences even in the active space and basis set can produce a significant change in the calculated S_2 barrier. This is one of the reasons leading to different levels of S_2 trapping in the earlier CASSCF simulations.^{20,25–27}

Here, in this study, we want to investigate how the dynamics are effected by the underlying electronic structure theory and if there is any trapping on the S_2 state at higher levels of theory than CASSCF. Hence, we perform non-adiabatic excited state dynamics simulations of uracil using trajectory surface hopping (TSH) methodology on potential energy surfaces (PES) calculated at CASSCF, MRCI with single excitations (MRCIS) and extended MS-CASPT2 (XMS-CASPT2) levels to investigate the effect of dynamic correlation on the relaxation of uracil. Dynamics are also carried out at the time dependent density functional theory (TD-DFT) level for an overall comparison to the multi-reference ab initio electronic structure theory levels. Since we are interested in the effects of electron correlation on the dynamics, the active space and basis set are kept the same for all the multi-reference theory levels. This study only considers the lowest three singlet states of uracil. Triplet states can arguably be involved in the dynamics of uracil to some extent as shown by Richter et al.,²⁸ but we have not considered them here, as performing all these simulations with both singlet and triplet states would be computationally prohibitive at the aforementioned high-levels of theory, and also the intersystem crossing dynamics is not the focus of our work.

2 Computational Methods

2.1 Electronic Structure Calculations

The ground state of the biologically relevant tautomer of uracil (shown in Figure 1(a)) was optimized at density functional theory (DFT)^{34,35} level using the B3LYP^{36–39} functional and 6-31G(d)⁴⁰ basis set using the Gaussian09 package.⁴¹ The frequencies were calculated at the same level of theory to ensure that the optimized geometry is the desired minimum. The multi-reference theory levels that we selected for our study are the CASSCF,⁴² MRCIS,⁴³ and XMS-CASPT2.^{44–46} The active space employed was 12 electrons in 9 orbitals and three states were averaged. The active space employed in this study which consists of 3 pairs of π and π^* orbitals, both out-of-plane lone-pairs of the N atoms, and the in-plane lone pair of O8, is shown in Figure 1(b). The MRCIS and XMS-CASPT2 calculations were performed using the corresponding CASSCF reference wavefunction. In addition, for the XMS-CASPT2 calculations, the single-state single-reference (SS-SR) contraction scheme⁴⁷ and an imaginary shift of 0.2 a.u. (to avoid intruder states) were employed. The TD-DFT^{48–50} level was also selected for an overall comparison with the multi-reference methods. Dunning type⁵¹ cc-pVDZ basis set was used for the multi-reference methods and Pople type 6-31G(d) basis set was used for the TD-DFT method with a B3LYP functional. Vertical excitation energies (VEE) and oscillator strengths were calculated at all levels of theory.

Conical intersections between S_2 and S_1 state (CI21) were located for all levels of theory. The S_2 minimum (S_2 min) and S_2 transition state (S_2 TS) were also located at CASSCF, MR-CIS, TD-DFT levels. Linear interpolations in internal coordinates (LIIC) were performed from the Franck-Condon (FC) point to CI21 for all the methods (including S_2 min and S_2 TS, at CASSCF and MRCIS levels) to calculate the shape of the potential energy surface (PES) at all levels of theory. All CASSCF and MRCIS calculations have been performed with the Columbus 7.0^{52–54} package, whilst the XMS-CASPT2 calculations have been performed with the Bagel package.^{55,56} TD-DFT single point (SP) calculations were performed with Gaussian09 package, while the CI21 optimizations were performed with QChem⁵⁷ at the TD-DFT level with Tamm-Dancoff approximation (TD-DFT/TDA). The CI21 optimizations at TD-DFT/TDA level did not converge and hence, we had to select the geometries for which the difference in energies between S_2 and S_1 were least (0.0068 eV for the ethylenic CI and 0.0407 eV for the ring-opening CI). The ethylenic CI between S_1 and S_0 (CI10) has also been optimized at the multi-reference levels.

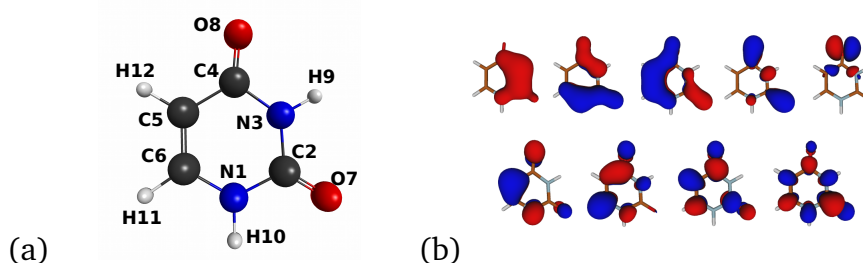


Fig. 1 (a) Uracil FC geometry with the conventional atom numbering which will be used throughout the paper. (b) Active space used in this study comprising of 12 electrons in 9 orbitals.

2.2 Trajectory Surface Hopping Dynamics

Sampling was performed using a harmonic oscillator Wigner distribution in Newton-X 2.0^{58,59} to generate initial conditions (nuclear coordinates and velocities) based on the optimized geometry and the normal modes from the B3LYP/6-31G(d) calculation, at 298 K. 500 initial conditions were generated for CASSCF and MRCIS levels, and 1000 initial conditions for TD-DFT level. For XMS-CASPT2 level, the same 500 initial conditions as MRCIS were selected. The S_1 and S_2 VEEs and oscillator strengths of uracil for the 500 geometries were calculated at all three multi-reference levels of theory using the cc-pVDZ basis set with an active space of 12 electrons in 9 orbitals. The S_1 and S_2 VEEs and oscillator strengths for 1000 geometries of uracil were also calculated at the TD-DFT level using the B3LYP functional and 6-31G(d) basis set. The vertical excitation energies and oscillator strengths were used to calculate the absorption cross sections to simulate the first absorption band of uracil for all methods. A Lorentzian line shape with a phenomenological broadening (δ) value of 0.1 eV for TD-DFT and 0.2 eV for the multi-reference methods were employed. The XMS-CASPT2 absorption spectrum was plotted using our in-house code SARcASM.⁶⁰

We performed non-adiabatic excited state dynamics simulations using TSH in Newton-X on CASSCF(12,9)/cc-pVDZ, MRCIS/CAS(12,9)/cc-pVDZ, XMS-CASPT2/CAS(12,9)/cc-pVDZ, and TD-DFT/B3LYP/6-31G(d) full dimensional potential energy surfaces.^{61–67} The energy, gradients and couplings were calculated on-the-fly using the Columbus 7.0 (CASSCF and MRCIS), Bagel (XMS-CASPT2), and Gaussian09 (TD-DFT) packages. The dynamics for XMS-CASPT2 were performed using the updated version (2.2) of Newton-X⁶⁸ which includes the Bagel interface. The experimentally measured first absorption peak for uracil in the gas phase is at 5.08 eV (244 nm).⁶⁹ In pump-probe experiments, the pump pulse bandwidth is typically much narrower than the absorption spectrum of the molecule. We tried to mimic such a narrow pulse centered at 4.77 eV (260 nm), previously used in our pump-probe experiments on uracil,²⁹ which is 0.31 eV lower than the experimental maximum. Hence, 0.31 eV was subtracted from the peak of the theoretical spectrum at all levels of theory to estimate the center of the pump pulse. The first absorption peaks were calculated to be at 6.6, 5.9, 4.8 and 5.1 eV for CASSCF, MRCIS, XMS-CASPT2, and TD-DFT levels, respectively. The excitation windows were 6.29 ± 0.15 , 5.59 ± 0.15 , 4.49 ± 0.15 , and 4.79 ± 0.15 eV at the CASSCF, MRCIS, XMS-CASPT2 and TD-DFT levels, which selected 71, 73, 55, and 100 initial conditions, respectively, for trajectory propagation.

At the FC geometry, S_2 is the optically bright state for uracil at all levels of theory employed here. Hence, the trajectories were propagated starting from the S_2 state for CASSCF, MRCIS, and TD-DFT level for the selected initial conditions within the excitation window. However, a very small geometrical displacement can switch the state ordering when the excited states energies are in very close proximity to each other at the FC geometry. This is the case at the XMS-CASPT2 level for the initial conditions selected, where 36 of them have S_1 as the bright state and the rest 19 have S_2 as the bright state. Hence, 36 trajectories were propagated starting from the S_1 state and the rest from the S_2 state, for the XMS-CASPT2 level.

The fewest switches surface hopping (FSSH)⁷⁰ algorithm was used to take into account non-adiabatic events among S_2 , S_1 , and S_0 states. The FSSH algorithm was corrected for decoherence effects using the approach of non-linear decay of mixing by Granucci et al.⁷¹, keeping the parameter $\alpha = 0.1$ hartree (recommended).⁷² The velocity Verlet algorithm was employed to integrate Newton's equations of motion with a time step of 0.5 fs and the semiclassical time-dependent Schrödinger equation was integrated using fifth-order Butcher's algorithm with a time step of 0.025 fs. For all the multi-reference methods, in order to conserve the total energy/momentum at a hop, the energy was rescaled along the non-adiabatic coupling vector, whilst for TD-DFT, the energy has been rescaled along the total velocity vector. In addition, the momentum direction was left unaltered when a frustrated hop was encountered. A detailed discussion of how to deal with issues such as decoherence, energy/momentum rescaling at a hop, frustrated hops etc. can be found elsewhere.^{73,74} For the TD-DFT dynamics, the coupling between S_1 and S_0 is not properly calculated, which is why, there are no S_1/S_0 hops. Instead, the trajectories are stopped

when the energy difference between S_1 and S_0 becomes < 0.2 eV. These are the only trajectories, which can be considered to populate S_0 , at the TD-DFT level. The TSH simulations were performed for 1000 fs at the CASSCF and TD-DFT level, 500 fs at the MRCIS level and 300 fs at XMS-CASPT2 level (MRCIS and XMS-CASPT2 being computationally expensive) using XSEDEs computational resources⁷⁵. Kinetic models to the populations were fitted using an auxiliary script available in SHARC 2.0 package.⁷⁶ The TSH simulations with multi-reference methods often lead to trajectories that crash or fail due to active space/energy conservation failure. A discussion of how this has been dealt with for population analysis has been provided in the Electronic Supplementary Information (ESI)[†].

3 Results and Discussion

3.1 Vertical Excitation Energies and Oscillator Strengths

We report the vertical excitation energies and oscillator strengths of uracil at the FC geometry (optimized at B3LYP/6-31G(d) level) at all the four levels of theory that has been employed for on-the-fly PES generation in dynamics, in Table 1. At all four levels of theory, S_1 is found to be a dark, $n_o\pi^*$ state and S_2 , a bright, $\pi\pi^*$ state, which has been established before, in a multitude of studies.^{3,19,77–82} The bright S_2 state with a value of 5.04 eV at the XMS-CASPT2/CAS(12,9)/cc-pVDZ level is the closest to the experimental first absorption peak. All other methods overestimate the energy of the bright state at the FC geometry, especially the multi-reference methods CASSCF and MRCIS. The CASSCF method does not include any treatment of dynamic electron correlation. It has the ability to only treat static electron correlation and hence, typically overestimates the vertical excitation energies of the neutral excited states by a substantial amount. Here, at CASSCF(12,9)/cc-pVDZ level, the bright state is situated at 6.67 eV, overestimated by 1.59 eV compared to the experimental value. As MRCIS method treats the dynamic correlation partially by including only single excitations (from the active space only) amongst the CASSCF configuration state functions (CSFs), it reduces the overestimation of energy to some extent, without being able to recover the total correlation energy. Hence, MRCIS/CAS(12,9)/cc-pVDZ also overestimates the bright state (6.12 eV) energy, albeit not as much as CASSCF, but by 1.04 eV. XMS-CASPT2, on the other hand, treats dynamical correlation by including second-order perturbation. Compared to the multi-reference methods, TD-DFT method is quite different. In TD-DFT, the exact form of the dynamic correlation is known, but the exact form of exchange correlation is not available, and depends on the specific functional being used. The B3LYP functional used here includes the exact Hartree-Fock (HF) exchange mixed with 3 of Becke's parameters to model the exchange part. TD-DFT/B3LYP/6-31G(d) level only overestimates the bright state energy (5.31 eV) by 0.23 eV, performing better than CASSCF and MRCIS levels. The best estimates of the vertical excitation energies of the lowest two singlet states has been calculated to be 5.00 eV and 5.25 eV, using completely renormalized EOM-CCSD with perturbative triples [CR-EOM-CCSD(T)] correction to account for dynamic correlation, coupled to an aug-cc-pVTZ basis set.⁷⁷ MS-CASPT2⁸² and

SS-CASPT2^{79,81} methods have also been found to produce the energies of the two lowest singlet states, very close to the CR-EOM-CCSD(T) values, with MS-CASPT2/CAS(14,10)/6-31G(d,p) estimating S_1 and S_2 energies as 4.93 and 5.18 eV, respectively.

Table 1 Vertical excitation energies and oscillator strengths (f) at different levels of theory. S_1 is a dark, $n\pi^*$ state and S_2 is the bright, $\pi\pi^*$ state. The experimental first absorption peak value has been taken from ref.⁶⁹

Method	E(S_1)/eV (f)	E(S_2)/eV (f)	ΔE /eV
CASSCF	5.04 (5.1e−4)	6.67 (0.40)	1.63
MRCIS	5.24 (1.9e−4)	6.12 (0.25)	0.88
XMS-CASPT2	4.86 (7.4e−5)	5.04 (0.27)	0.18
TD-DFT	4.67 (1.0e−4)	5.31 (0.12)	0.64
Expt.		5.08	

Comparing all the methods employed in this study with the experimental peak and the computational best estimates of the lowest singlet states, it is easy to assess that XMS-CASPT2/CAS(12,9)/cc-pVDZ level has delivered better results in reproducing the energies of S_1 and S_2 states at the FC geometry of uracil. The $S_1 - S_2$ energy gap (0.18 eV) for this level of theory is also very similar to the computational best estimates (0.25 eV) mentioned before, albeit slightly smaller than them. This could be an effect of using a small basis set, since there is a possibility of strong basis set dependence. Nonetheless, XMS-CASPT2 with cc-pVDZ basis set agrees very well with the best estimates and it is not possible to use a larger basis set for the dynamics due to the computational cost. The main goal is to understand the effect of electron correlation or electronic structure methods on the relaxation dynamics of uracil. Thus, the basis set has been kept the same for the multi-reference methods.

3.2 Absorption Spectra

Figure 2 shows the normalized absorption spectra (specifically the first absorption band) simulated at all levels of theory overlaid with the normalized experimental first absorption band. As can be seen from this figure, the first absorption peaks are at 6.6, 5.9, 4.8 and 5.1 eV at the CASSCF, MRCIS, XMS-CASPT2, and TD-DFT levels, respectively. The first absorption peak is overestimated at the CASSCF and MRCIS levels by 1.8 and 1.1 eV, respectively. This behavior is very typical of the aforementioned levels of theory as discussed before in section 3.1. The absorption peak at the XMS-CASPT2 level is 0.28 eV red-shifted from the experimental peak. The TD-DFT peak is almost overlapping with the experimental peak having a blue shift of only 0.02 eV. This is very intriguing since the VEE of S_2 at the XMS-CASPT2 level was the closest to the absorption peak, and not the TD-DFT S_2 energy. Comparing the S_2 energies at the FC geometry from Table 1 to the first absorption peaks at all levels of theory, it is easy to observe that the calculated absorption peak is red-

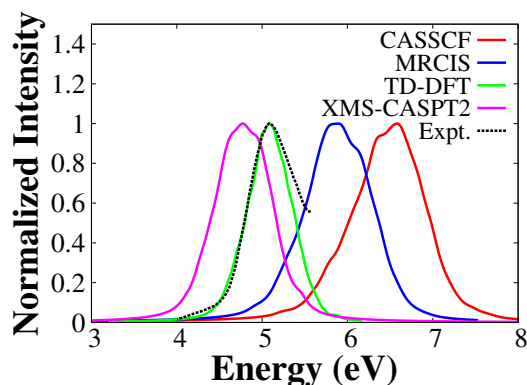


Fig. 2 Normalized absorption spectrum (first absorption band) at CASSCF, MRCIS, XMS-CASPT2 and TD-DFT level overlaid with the experimental first absorption band taken from ref.⁶⁹.

shifted compared to the calculated VEE of S_2 at the FC geometry, which suggests that the experimental absorption maximum may not correspond to the VEE of the bright S_2 state because of the FC factors. When the calculated absorption spectra at different levels of theory are compared, TD-DFT performs better than all the multi-reference levels of theory, being able to both predict the peak and the shape of the peak. Nonetheless, XMS-CASPT2 agrees better with the experimental absorption peak compared to the other multi-reference methods.

A previous study suggested that the S_3 excited state may contribute to the absorption spectrum, although the degree of contribution was very sensitive to the level of theory.²⁸ In this study we did not include the S_3 state. Since the excitation of the pump laser we are trying to simulate is on the red side of the spectrum (at 260 nm), we expect that the contribution of the S_3 state on the dynamics initiated with such excitation to be small.

3.3 Conical Intersections

Figure 3 shows all the minimum energy CIs that we have optimized. In case of the multi-reference methods, we have only optimized the ethylenic CIs, since they are the most crucial ones in our dynamics. For TD-DFT/TDA level, we localized the ethylenic and ring-opening CI for the S_2/S_1 seam. We were not able to locate the ring-opening CI for the multi-configurational multi-reference methods, since the active space employed in our study does not comprise of any σ or σ^* orbital along N3-C4 bond. A detailed discussion about all the different CIs of uracil can be found elsewhere.²⁵ By analyzing the time-evolution of twist around the C5=C6 bond and pyramidalization at C5 in our simulations, which will be discussed later in section 3.6, we have found that the ethylenic CIs dominate internal conversion of uracil at earlier delays. Therefore, we mainly focus on the ethylenic CIs.

The ethylenic CI21 at the CASSCF and MRCIS levels are very similar. In both cases, the C5=C6 and C4=O8 bonds stretch quite a lot (and C4-C5 contract as a result) along

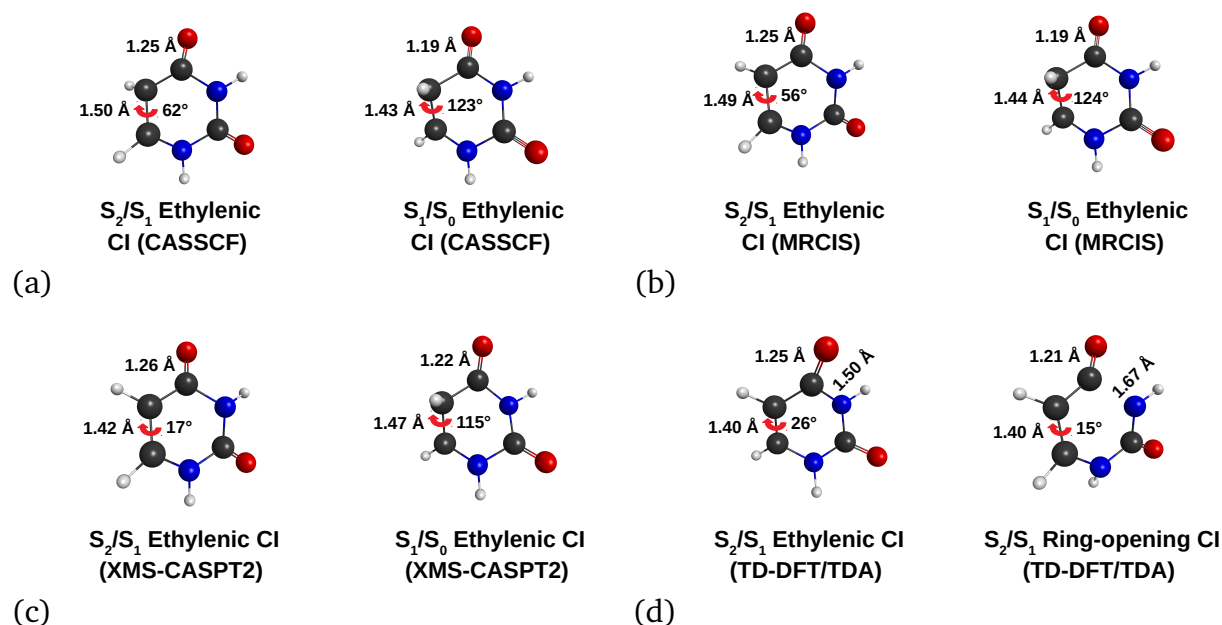


Fig. 3 Optimized CIs at the (a) CASSCF, (b) MRCIS, (c) XMS-CASPT2, and (d) TD-DFT/TDA levels of theory. For further details about the structures and Cartesian coordinates, refer to the SI.

with a very similar twist of C5=C6 bond and a slight pyramidalization of C5. The XMS-CASPT2 ethylenic CI21, on the other hand, has very small deviation from planarity and is located very close to the FC geometry, since the energy gap between S_2 and S_1 is very small at the FC region. The ethylenic CI10 is very distinct from the ethylenic CI21, since it largely deviates from planarity. For all CASSCF, MRCIS, and XMS-CASPT2 levels, this CI has a large twist around the C5=C6 bond and the C5 is substantially pyramidalized. The ethylenic CI21 at the TD-DFT/TDA level is also quite close to the FC geometry like the XMS-CASPT2 one, and also has the C5=C6 and C4=O8 bonds stretched compared to the FC geometry. On the other hand, the ring-opening CI21 at the TD-DFT/TDA level has a really elongated N3-C4 bond along with a stretched C5=C6 bond, while the C4=O8 is not stretched. Information about other important internal coordinates and the energies of these CIs can be found in the ESI.[†]

3.4 Investigation of the Barrier on the S_2 Surface

There have been many studies that investigated the PES of uracil after photo-excitation to the bright S_2 state. It has been found that the S_2 PES of uracil can be quite different depending on the level of theory being employed. Previous results from the literature, together with our current results are presented together in Table 2. Negative barriers (negative barriers are obtained when a transition state geometry that has been optimized at a lower level of theory is used to calculate the energy of the barrier at a higher level of theory) mean the pathway is essentially barrierless. It can be seen from Table 2 that

the barrier on S_2 ranges from <0.02 to 0.88 eV. This has become a contentious topic since the excited population on the S_2 surface might decay faster or slower depending on the size of the barrier. The size of the barrier on the S_2 state typically decreases substantially in going from CASSCF to higher level multi-reference and single reference theories. The barrier changes significantly even when the state-averaging, active space, and basis set are changed at the CASSCF level. It has been claimed that this barrier will be insignificant in dynamics, given the amount of energy the system acquires during excitation.²⁵ However, there has been no dynamics study on uracil using a PES at a higher level of electronic structure theory than CASSCF, to the best of our knowledge. As we will see later in section 5, the barrier definitely has a distinctive effect on the S_2 decay. The barrier has also been provided for the level of theories that we have used for our dynamics simulations. It can be seen from Table 2 that MRCIS and XMS-CASPT2 have almost negligible barriers while CASSCF does not. Hence, it is expected that a population trap on the S_2 state will slow the decay of that state for CASSCF method, while that will not occur for the other methods.

Table 2 Barrier on the S_2 state of uracil at different levels of theory. These values are taken from literature or calculated by us using 3 state averaging and cc-pVDZ basis set for the multi-reference methods, and 6-31G(d) basis set for TD-DFT method. Negative barriers may be obtained when a geometry that has been optimized at a lower level of theory (see Ref.¹⁷) is used to calculate the barrier at a higher level of theory. Whenever the S_2 TS was not optimized, we have indicated that with an inequality to show that it is an upper bound for the barrier.

Method	Barrier on S_2 /eV
SA-3-CASSCF(12,9)/6-311+G(d) ref. ¹⁷	0.31
MRCI/CAS(12,9)/6-311+G(d) ref. ¹⁷	-0.09
EOM-CCSD/6-311+G(d) ref. ¹⁷	-0.13
SA-3-CASSCF(8,6)/6-31G(d) ref. ²⁰	0.26
SA-5-CASSCF(8,7)/6-31G(d) ref. ²⁰	0.88
SA-5-MSPT2/CAS(8,7)/6-31G(d) ref. ²⁰	0.17
MS-CASPT2(12,9)/DZP ref. ³³	<0.02
CASSCF(12,9)	0.16
MRCIS/CAS(12,9)	0.03
XMS-CASPT2/CAS(12,9)	<0.02
TD-DFT/B3LYP	<0.03

Figure 4 shows all the LIICs that have been performed to give a simple representation of the PES of uracil on the S_2 surface from FC geometry to S_2/S_1 ethylenic CI.

3.5 Dynamics

Figure 5 shows the normalized population dynamics of uracil for S_2 , S_1 and S_0 states at all levels of theory. It is relatively easy to recognize that the dynamics is quite distinctive

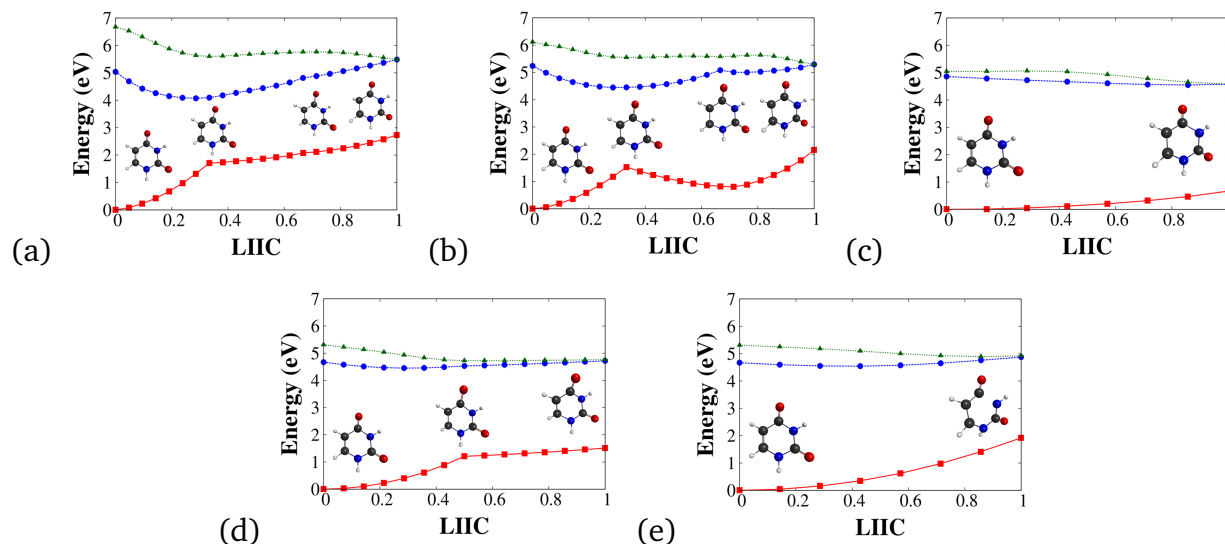


Fig. 4 Linear Interpolation from FC to ethylenic CI21 at (a) CASSCF (b) MRCIS (c) XMS-CASPT2, and (d) TD-DFT level. (e) represents LIIC to the ring-opening S_2/S_1 CI at TD-DFT level. In all the panels, the red-solid line, the blue-dashed line and the green-dotted line represents the S_0 , S_1 and S_2 states, respectively.

for each level of theory, especially for the multi-reference levels. The S_2 state population decays, completely, quite rapidly for MRCIS and XMS-CASPT2 levels, while $\sim 20\%$ population is still remaining in the S_2 state at 1000 fs for CASSCF level. S_2 decay at the TD-DFT level is also quite fast, but not as rapid as the decays at the MRCIS and XMS-CASPT2 levels. It is known that in uracil, as S_2 decays, the population on the S_1 surface either relaxes via the $\pi\pi^*/$ closed shell pathway rapidly to reach the S_1/S_0 CI directly or gets trapped in the dark $n\pi^*$ state and relaxes to the ground state *via* the $n\pi^*/$ closed shell pathway. A signature of this can be observed very clearly for the MRCIS and XMS-CASPT2 dynamics. In MRCIS dynamics, the population on the S_1 and S_0 state both start to increase rapidly with S_2 decay, S_1 more than S_0 . That rapid gain of population ceases somewhere between 100-150 fs, evidenced by the sudden change of the slope of the population on both surfaces, and henceforth, S_0 state gains population very slowly from the S_1 state. A very similar situation is visible for XMS-CASPT2 dynamics too. Only in this case, the population is on both S_1 and S_2 states, initially. Hence, the S_1 state gains population rapidly from S_2 and then starts losing population to S_0 rapidly till ~ 150 fs. After 150 fs, the population exchange between S_1 and S_0 becomes very slow. For both of these methods, the relaxation is dominated by the $\pi\pi^*/$ closed shell pathway for the first ~ 150 fs, and then the population gets trapped on the dark S_1 state. The MRCIS and XMS-CASPT2 dynamics show no trapping at all on the S_2 surface, as is expected from the barrier height on S_2 . However, in case of CASSCF dynamics, the increase in the S_0 population is very gradual, as is the decay in S_2 , for the whole simulation window. This is probably due to trapping of a significant portion of the

population on the S_2 state, since there is a substantial barrier on S_2 at the CASSCF level on the way to the ethylenic CI21, compared to the higher level multi-reference methods. As a consequence, the S_2 decay becomes much slower at the CASSCF level. At the TD-DFT level, population decay looks very similar to the MRCIS population decay i.e. it shows very little to no evidence of S_2 trapping. However, it is somewhat slower than MRCIS, but much faster than CASSCF. Also, the decay of the S_1 state after about 300 fs is much faster in case of TD-DFT than MRCIS. Nonetheless, the TD-DFT dynamics pathway has been found to be completely different than the multi-reference levels, since all the trajectories that are considered to be on the ground state, are there due to ring-opening *via* N3-C4 bond cleavage. This will be discussed in detail later.

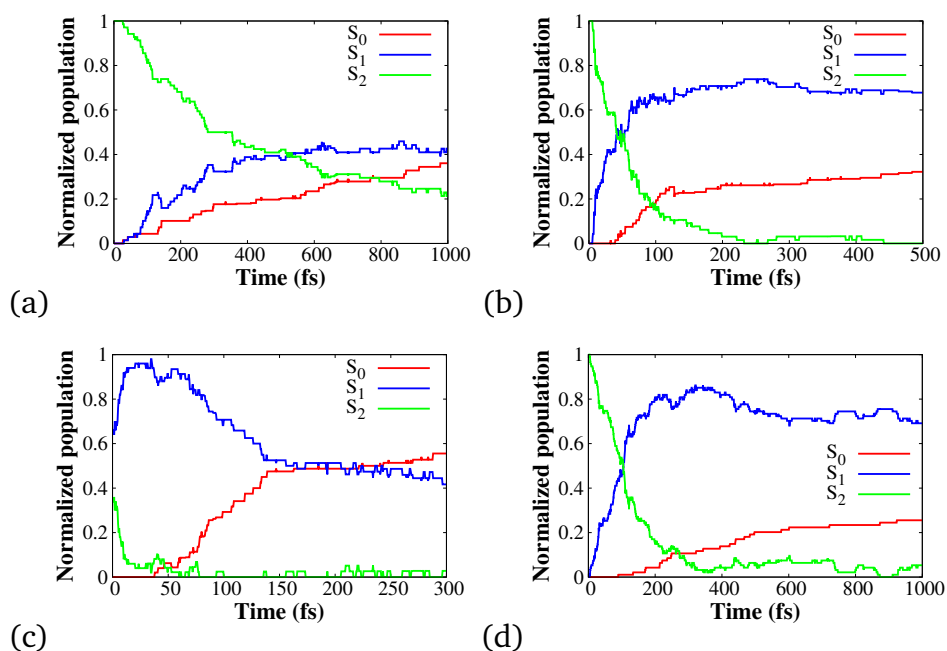


Fig. 5 Normalized population dynamics for the lowest three singlet states (S_2 , S_1 and S_0) of uracil at the (a) CASSCF, (b) MRCIS, (c) XMS-CASPT2, and (d) TD-DFT level.

We have fitted two types of kinetic models to the populations, and the results are all provided in the ESI.[†] Since the kinetic models are problematic (other than the S_2 fits), here we only report the S_2 lifetimes with a mono-exponential decay function (refer to consecutive fits in the ESI[†]). The lifetimes that were obtained for the S_2 decay are 575.5, 66.0, 12.5, 129.0 fs at the CASSCF, MRCIS, XMS-CASPT2 and TD-DFT level, respectively. This clearly demonstrates how rapid the population on S_2 decays for MRCIS, XMS-CASPT2 and TD-DFT levels, while the CASSCF S_2 lifetime is almost 5 times larger than the slowest of the former three methods, suggesting a substantial trap on the CASSCF S_2 surface, as has been predicted by the barrier calculations. Most of the experiments that have been performed on uracil have found two timescales in the ultrafast regime: one of the order of <200 fs and the other between 2-3.3 ps.^{9,13-18} Only Ulrich *et al.* have found an intermedi-

ate timescale of 530 fs in addition to the aforementioned shorter and longer timescales.¹⁰ Some of the previous dynamics studies based on CPMD/BLYP, OM2/MRCI and CASSCF PESs, have found one timescale in this intermediate range, for the decay of S_2 , similar to our CASSCF S_2 lifetime.^{21,23,25,27} In our calculation, none of the methods other than CASSCF can recover the intermediate timescale. Rather, they all show a rapid S_2 decay, with a very short timescale, in accordance with the short timescale of most of the experimental studies. This suggests that there is negligible or no trapping on the S_2 surface at the higher levels of theory.

As our kinetic model fits did not work well, especially for S_0 , we did not try to compare the longer timescales generated by these fits to the experimental ones. Also, none of our simulations windows go anywhere near the longer timescale, due to current computational constraints. On top of that, there are only a few trajectories with S_1/S_0 hops after ~ 150 fs at the MRCIS and XMS-CASPT2 levels, and none of the hops represent an $n\pi^*$ /closed shell CI seam. It would not be correct to model the fate of the population trapped on the $n\pi^*$ state considering the aforementioned points.

3.6 Time-evolution of Internal Coordinates

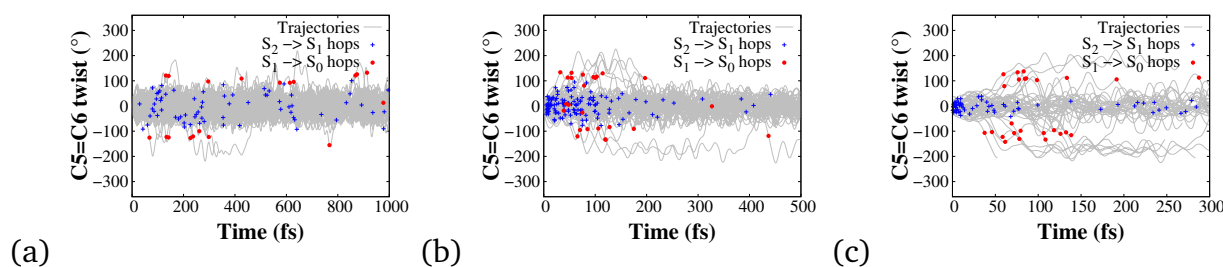


Fig. 6 Time-evolution of the twist around C5=C6 bond (dihedral angle H12-C5=C6-H11) at (a) CASSCF, (b) MRCIS, and (c) XMS-CASPT2 level. The blue and the red dots represent the $S_2 \rightarrow S_1$ hops and $S_1 \rightarrow S_0$ hops, respectively, along the trajectories.

Figure 6 shows the time-evolution of the twist around C5=C6 bond for all the multi-reference methods, along with the $S_2 \rightarrow S_1$ hops and $S_1 \rightarrow S_0$ hops, for all trajectories. This clearly demonstrates that the hops occur along the ethylenic CI seams (both for S_2/S_1 and S_1/S_0 seams) for most of the trajectories for all the multi-reference methods. The values of the twist angle are shown in Figure 3 and ESI (Table 1)[†], they are around 60° for the S_2/S_1 (except XMS-CASOT2 which is 17°), and they increase to 110 - 120° at the S_1/S_0 CI. Figure 6 shows the hops occurring around these values, especially the S_1/S_0 hops. This figure also goes on to show the clear demarcation between the two different seams: S_2/S_1 and S_1/S_0 . In spite of relaxing through the ethylenic CIs, the two seams are quite different which has also been discussed in the previous section. The S_2/S_1 CI has a smaller ethylenic twist compared to the S_1/S_0 CI at all levels of theory, especially, XMS-CASPT2 level. The distinction between the two seams is also more prominent for the XMS-CASPT2

level of theory, since the S_2/S_1 CI has a very small twist and all the S_2/S_1 hops are quite localized around that CI in a range of $0-50^\circ$, whilst the S_1/S_0 hops have twists larger than 80° . Although the distinction is also fairly clear in case of CASSCF and MRCIS dynamics, the range of the S_2/S_1 twist is not as localized for these levels as XMS-CASPT2, having a range between $0-90^\circ$. There are a few S_1/S_0 hops which are visible for mainly MRCIS level, which are further away from the ethylenic S_1/S_0 CI seam and have small twist values. These are the few trajectories in MRCIS method that relax through the N3-C4 ring-opening coordinate. C5=C6 twisting itself is not enough to reach CI. Pyramidalization of one of the carbons is also necessary and in this case, C5 pyramidalizes to facilitate the process. Similar plots like Figure 6 are provided for C5 and C6 pyramidalization in the SI that show how distinct the S_2/S_1 and S_1/S_0 seams are in case of C5 pyramidalization, and not for C6 pyramidalization.

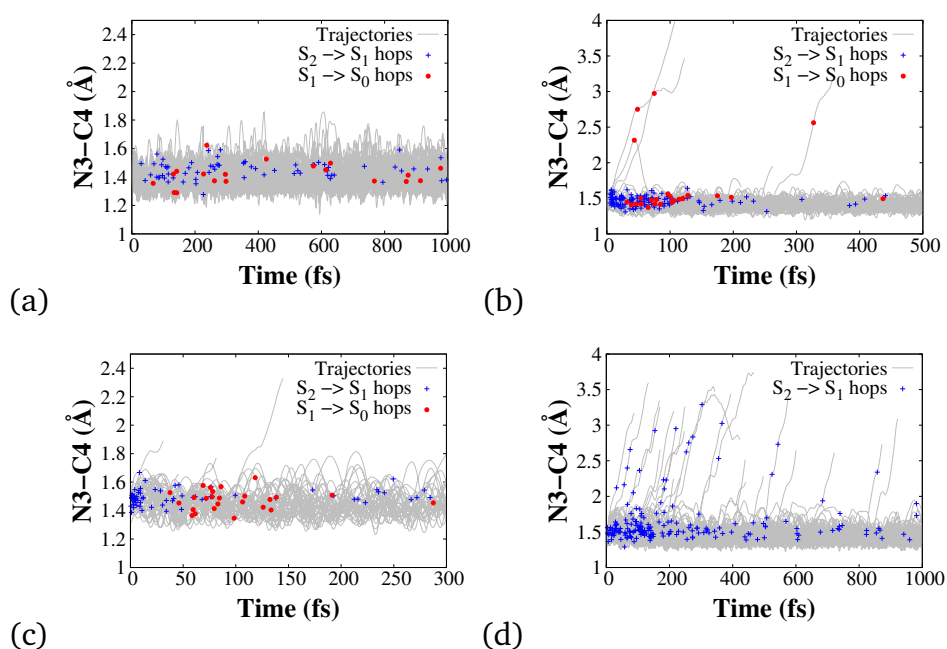


Fig. 7 Time-evolution of N3-C4 bond to show ring-opening pathway at (a) CASSCF, (b) MRCIS, (c) XMS-CASPT2, and (d) TD-DFT level.

Figure 7 shows the time-evolution of N3-C4 bond for all the methods. This figure demonstrates clearly the contribution of the ring-opening coordinate in the relaxation process. Although this pathway has been found to contribute in earlier dynamics studies with CASSCF PES,^{25,28} we have not found any evidence of this pathway in our CASSCF dynamics. However there is evidence of this pathway in all other methods, albeit to a very small extent in MRCIS and XMS-CASPT2. In MRCIS dynamics, there are four trajectories where the S_1/S_0 hops occur on the elongated N3-C4 bond. However, only 3 of them actually go through the bond breaking process. This is visible in the Figure 7b) quite clearly. Although we do not see any hops through the ring-opening coordinate in XMS-CASPT2 dynamics,

we do see a few trajectories where the N3-C4 bond elongates and the trajectories fail due to active space deterioration. No S_2/S_1 hops exist on the elongated N3-C4 coordinate for the multi-reference electronic structure methods. Nonetheless, this completely changes in case of the TD-DFT dynamics. The N3-C4 bond elongates for a lot of trajectories in this case. Actually, all the trajectories that are considered to be on the ground state relax *via* the N3-C4 bond elongation process. We can also see that the S_2/S_1 hops are also located on the elongated N3-C4 bond, in case of TD-DFT dynamics. This has very serious implications because this would mean that a huge portion of trajectories go through a photochemical reaction, instead of coming back to the ground state of uracil, which would mean uracil is not photostable. There has been an experimental study where the authors observed ring opening after UV irradiation of nucleosides in DNA only.⁸³ Even then, the isocyanates (R-N=C=O) detected cannot form directly from the N3-C4 bond cleavage. More recently, Ghafur et al. used their newly built ultra-high vacuum spectrometer incorporating a laser-based thermal desorption source and performed time-resolved ion-yield measurements for uracil, exciting at 267 nm, which provided no evidence for the appearance of the fragment with mass/charge ratio of 84 (which has, previously, been interpreted as a signature of a ring-opening process in ultraviolet nanosecond laser excitation at wavelengths ≤ 232 nm)⁸⁴ within the first few hundred picoseconds following excitation.¹⁸

The other motions that are important during the relaxation process are the stretching and contracting of some of the important bonds of uracil. Specifically, we investigated the C5=C6 and C4=C8 bonds, both of which are stretched at the S_2 min and the S_1 min, compared to the FC geometry. The stretching of the C4=O8 bond has also been used in ultrafast X-ray Auger probing of the photoexcited dynamics of DNA pyrimidine nucleobase thymine (which has a methyl group instead of a H at C5 for uracil) to demonstrate that the initially excited $\pi\pi^*$ state relaxes to the dark $n\pi^*$ state within 200 fs.⁸⁵ More recently, near-edge soft X-ray absorption spectroscopy has been employed at the oxygen K-edge to show that this internal conversion takes place in 60 ± 30 fs in thymine.⁸⁶ Transient X-ray absorption spectral fingerprints have also been computed to show the involvement of dark $n_o\pi^*$ state during photodynamics of uracil using C, N and O K-edge.⁸⁷ We included a discussion about the time-evolution of the ensemble average of the C5=C6 and C4=O8 bonds, for all the multi-reference methods, in the ESI[†].

Both Figure 6 and 7 also give us temporal information about the hops which can be corroborated with the population plots. For MRCIS and XMS-CASPT2, it is clear that most of the S_1/S_0 hops occur before ~ 150 fs. This explains the rapid rise in the S_0 population in both levels of theory before 150 fs. There are always multiple hops back and forth between S_2 and S_1 , which makes things more complicated. But, most of the S_2/S_1 hops also occur before 100 fs for MRCIS and 50 fs for XMS-CASPT2, which explains the rapid increase of S_1 , too, between 0-100 fs and 0-50 fs, for MRCIS and XMS-CASPT2, respectively. This is also an evidence that there is almost negligible population trap on the S_2 state for MRCIS and XMS-CASPT2 dynamics. After 150 fs, the population mostly gets trapped in the dark

$n\pi^*$ state and very few S_1/S_0 hops occur during the simulations window, which is evidenced by the gradual rise of S_0 population and gradual decay of S_1 population after 150 fs, for both MRCIS and XMS-CASPT2. However, the same cannot be observed for CASSCF, where the hops are quite uniformly distributed between 0-1000 fs. This explains the gradual rise of S_1 (and later decay) and S_0 population for the CASSCF dynamics and is also an evidence of a population trap on both the S_2 and S_1 state.

4 Conclusion

In this study, we have performed non-adiabatic excited state dynamics simulations of uracil at different electronic structure theory levels to understand how the dynamics are influenced by electron correlation (especially, dynamic electron correlation), and to gain an insight into the much debated population trapping on the S_2 state. Our results suggest that there is no trapping of population on the S_2 state at higher-level multi-reference methods (MRCIS and XMS-CASPT2) and at TD-DFT/B3LYP level, whereas there is substantial trapping of population on the S_2 state at the CASSCF level, as is suggested by the size of the barrier on S_2 at different levels of theory. TD-DFT/B3LYP, however, can not treat exchange correlation and static correlation properly, and the dynamics, in this case, rather, proceed *via* a ring-opening pathway which would create photochemical products. There has not been any convincing evidence of this pathway experimentally, and this pathway is only observed in very few trajectories at the MRCIS level. Theoretically, including dynamic correlation (in addition to static correlation) of electrons is very significant in modelling accurate PESs. Hence, these results indicate that decay from S_2 occurs very fast without substantial trapping. Experimental probes that clearly distinguish between the S_1 and S_2 signals will be very helpful in unequivocally demonstrating this process. Theoretically, longer timescale simulations in-conjunction with machine learning based PESs at the aforementioned higher levels of theory could be pursued in future to investigate the fate of the trapped $n\pi^*$ population and the source of the longer experimental timescale in the ultrafast regime.

Conflicts of interest

There are no conflicts to declare.

Acknowledgements

The authors gratefully acknowledge the Department of Energy (DOE, Award No. DE-FG02-08ER15983 for P.C. and S.M. and DOE, Award No. DE-FG02-08ER15984 for Y.L. and T.W.) for funding. Most of the computational work was performed using the Extreme Science and Engineering Discovery Environment (XSEDE), which is supported by National Science Foundation Grant No. ACI-1548562. P.C. thanks Asst. Prof. Jae Woo Park and XSEDE personnel for technical advice/help with running jobs and installation of Bagel package, and Dr. Sebastian Mai for general advice on trajectory surface hopping.

References

- 1 C. E. Crespo-Hernández, B. Cohen, P. M. Hare and B. Kohler, *Chem. Rev.*, 2004, **104**, 1977–2020.
- 2 C. T. Middleton, K. de La Harpe, C. Su, Y. K. Law, C. E. Crespo-Hernández and B. Kohler, *Ann. Rev. Phys. Chem.*, 2009, **60**, 217–239.
- 3 R. Improta, F. Santoro and L. Blancafort, *Chem. Rev.*, 2016, **116**, 3540–3593.
- 4 *Topics in Current Chemistry - Photoinduced Phenomena in Nucleic Acids I*, ed. S. Ullrich, A. C. Borin and M. Barbatti, Springer, Berlin - Heidelberg, 2015, vol. 355.
- 5 *Topics in Current Chemistry - Photoinduced Phenomena in Nucleic Acids II*, ed. S. Ullrich, A. C. Borin and M. Barbatti, Springer, Berlin - Heidelberg, 2015, vol. 356.
- 6 T. Gustavsson, R. Improta and D. Markovitsi, *J. Phys. Chem. Lett.*, 2010, **1**, 2025–2030.
- 7 P. M. Hare, C. E. Crespo-Hernandez and B. Kohler, *J. Phys. Chem. B*, 2006, **110**, 18641–18650.
- 8 P. M. Hare, C. E. Crespo-Hernandez and B. Kohler, *Proc. Natl. Acad. Sci.*, 2007, **104**, 435–440.
- 9 H. Kang, K. T. Lee, B. Jung, Y. J. Ko and S. K. Kim, *J. Am. Chem. Soc.*, 2002, **124**, 12958–12959.
- 10 S. Ullrich, T. Schultz, M. Z. Zgierski and A. Stolow, *Phys. Chem. Chem. Phys.*, 2004, **6**, 2796–2801.
- 11 Y. He, C. Wu and W. Kong, *J. Phys. Chem. A*, 2003, **107**, 5145–5148.
- 12 Y. He, C. Wu and W. Kong, *J. Phys. Chem. A*, 2004, **108**, 943–949.
- 13 C. Canuel, M. Mons, F. Piuze, B. Tardivel, I. Dimicoli and M. Elhanine, *J. Chem. Phys.*, 2005, **122**, 074316.
- 14 T. Gustavsson, Á. Bányász, E. Lazzarotto, D. Markovitsi, G. Scalmani, M. J. Frisch, V. Barone and R. Improta, *J. Am. Chem. Soc.*, 2006, **128**, 607–619.
- 15 T. Gustavsson, N. Sarkar, E. Lazzarotto, D. Markovitsi, V. Barone and R. Improta, *J. Phys. Chem. B*, 2006, **110**, 12843–12847.
- 16 M. Kotur, T. C. Weinacht, C. Zhou and S. Matsika, *IEEE J. Sel. Top. Quantum Electron.*, 2012, **18**, 187–194.
- 17 S. Matsika, M. Spanner, M. Kotur and T. C. Weinacht, *J. Phys. Chem. A*, 2013, **117**, 12796–12801.
- 18 O. Ghafur, S. W. Crane, M. Ryszka, J. Bockova, A. Rebelo, L. Saalbach, S. De Camillis, J. B. Greenwood, S. Eden and D. Townsend, *J. Chem. Phys.*, 2018, **149**, 034301.
- 19 S. Matsika, *J. Phys. Chem. A*, 2004, **108**, 7584–7590.
- 20 H. R. Hudock, B. G. Levine, A. L. Thompson, H. Satzger, D. Townsend, N. Gador, S. Ullrich, A. Stolow and T. J. Martínez, *J. Phys. Chem. A*, 2007, **111**, 8500–8508.
- 21 H. Nieber and N. L. Doltsinis, *Chem. Phys.*, 2008, **347**, 405–412.
- 22 N. L. Doltsinis, P. R. L. Markwick, H. Nieber and H. Langer, in *Ultrafast Radiationless*

- Decay in Nucleic Acids: Insights From Nonadiabatic Ab Initio Molecular Dynamics*, ed. M. K. Shukla and J. Leszczynski, Springer Netherlands, Dordrecht, 2008, pp. 265–299.
- 23 Z. Lan, E. Fabiano and W. Thiel, *J. Phys. Chem. B*, 2009, **113**, 3548–3555.
- 24 M. Barbatti, A. J. A. Aquino, J. J. Szymczak, D. Nachtigallová, P. Hobza and H. Lischka, *Proc. Natl. Acad. Sci.*, 2010, **107**, 21453–21458.
- 25 D. Nachtigallová, A. J. A. Aquino, J. J. Szymczak, M. Barbatti, P. Hobza and H. Lischka, *J. Phys. Chem. A*, 2011, **115**, 5247–5255.
- 26 B. P. Fingerhut, K. E. Dorfman and S. Mukamel, *J. Phys. Chem. Lett.*, 2013, **4**, 1933–1942.
- 27 B. P. Fingerhut, K. E. Dorfman and S. Mukamel, *J. Chem. Theory Comput.*, 2014, **10**, 1172–1188.
- 28 M. Richter, S. Mai, P. Marquetand and L. González, *Phys. Chem. Chem. Phys.*, 2014, **16**, 24423–24436.
- 29 S. L. Horton, Y. Liu, P. Chakraborty, P. Marquetand, T. Rozgonyi, S. Matsika and T. Weinacht, *Phys. Rev. A*, 2018, **98**, 053416.
- 30 H. Yu, J. A. Sanchez-Rodriguez, M. Pollum, C. E. Crespo-Hernández, S. Mai, P. Marquetand, L. González and S. Ullrich, *Phys. Chem. Chem. Phys.*, 2016, **18**, 20168–20176.
- 31 M. Etinski, T. Fleig and C. M. Marian, *J. Phys. Chem. A*, 2009, **113**, 11809–11816.
- 32 A. Yoshikawa and S. Matsika, *Chem. Phys.*, 2008, **347**, 393–404.
- 33 S. Yamazaki and T. Taketsugu, *J. Phys. Chem. A*, 2012, **116**, 491–503.
- 34 W. Kohn, A. D. Becke and R. G. Parr, *J. Phys. Chem.*, 1996, **100**, 12974–12980.
- 35 T. Ziegler, *Chem. Rev.*, 1991, **91**, 651–667.
- 36 A. D. Becke, *Phys. Rev. A*, 1988, **38**, 3098–3100.
- 37 C. Lee, W. Yang and R. G. Parr, *Phys. Rev. B*, 1988, **37**, 785–789.
- 38 S. H. Vosko, L. Wilk and M. Nusair, *Can. J. Phys.*, 1980, **58**, 1200–1211.
- 39 A. D. Becke, *J. Chem. Phys.*, 1993, **98**, 5648–5652.
- 40 R. Ditchfield, W. J. Hehre and J. A. Pople, *J. Chem. Phys.*, 1971, **54**, 724–728.
- 41 M. J. Frisch, G. W. Trucks, H. B. Schlegel, G. E. Scuseria, M. A. Robb, J. R. Cheeseman, G. Scalmani, V. Barone, B. Mennucci, G. A. Petersson, H. Nakatsuji, M. Caricato, X. Li, H. P. Hratchian, A. F. Izmaylov, J. Bloino, G. Zheng, J. L. Sonnenberg, M. Hada, M. Ehara, K. Toyota, R. Fukuda, J. Hasegawa, M. Ishida, T. Nakajima, Y. Honda, O. Kitao, H. Nakai, T. Vreven, J. A. Montgomery, J. E. Peralta, F. Ogliaro, M. Bearpark, J. J. Heyd, E. Brothers, K. N. Kudin, V. N. Staroverov, R. Kobayashi, J. Normand, K. Raghavachari, A. Rendell, J. C. Burant, S. S. Iyengar, J. Tomasi, M. Cossi, N. Rega, J. M. Millam, M. Klene, J. E. Knox, J. B. Cross, V. Bakken, C. Adamo, J. Jaramillo, R. Gomperts, R. E. Stratmann, O. Yazyev, A. J. Austin, R. Cammi, C. Pomelli, J. W. Ochterski, R. L. Martin, K. Morokuma, V. G. Zakrzewski, G. A. Voth, P. Salvador, J. J. Dannenberg, S. Dapprich, A. D. Daniels, O. Farkas, J. B. Foresman, J. V. Ortiz, J. Cioslowski and D. J. Fox, *Gaussian 09, Revision B.01*, 2009.

- 42 B. O. Roos, P. R. Taylor and P. E. Sigbahn, *Chem. Phys.*, 1980, **48**, 157 – 173.
- 43 R. J. Buenker and S. D. Peyerimhoff, *Theoret. chim. acta*, 1974, **35**, 33–58.
- 44 J. Finley, P.-Å. Malmqvist, B. O. Roos and L. Serrano-Andrés, *Chem. Phys. Lett.*, 1998, **288**, 299 – 306.
- 45 A. A. Granovsky, *J. Chem. Phys.*, 2011, **134**, 214113.
- 46 T. Shiozaki, W. Győrffy, P. Celani and H.-J. Werner, *J. Chem. Phys.*, 2011, **135**, 081106.
- 47 J. W. Park, *J. Chem. Theory Comput.*, 2019, **15**, 3960–3973.
- 48 E. Runge and E. K. U. Gross, *Phys. Rev. Lett.*, 1984, **52**, 997–1000.
- 49 R. Bauernschmitt and R. Ahlrichs, *Chem. Phys. Lett.*, 1996, **256**, 454 – 464.
- 50 F. Furche and R. Ahlrichs, *J. Chem. Phys.*, 2002, **117**, 7433–7447.
- 51 T. H. Dunning, *J. Chem. Phys.*, 1989, **90**, 1007–1023.
- 52 H. Lischka, R. Shepard, I. Shavitt, R. M. Pitzer, M. Dallos, T. Müller, P. G. Szalay, F. B. Brown, R. Ahlrichs, H. J. Böhm, A. Chang, D. C. Comeau, R. Gdanitz, H. Dachsel, C. Ehrhardt, M. Ernzerhof, P. Höchtl, S. Irle, G. Kedziora, T. Kovar, V. Parasuk, M. J. M. Pepper, P. Scharf, H. Schiffer, M. Schindler, M. Schüler, M. Seth, E. A. Stahlberg, J.-G. Zhao, S. Yabushita, Z. Zhang, M. Barbatti, S. Matsika, M. Schuurmann, D. R. Yarkony, S. R. Brozell, E. V. Beck, J.-P. Blaudeau, M. Ruckebauer, B. Sellner, F. Plasser and J. J. Szycmzak, *COLUMBUS, an ab initio electronic structure program, release 7.0 (2012)*.
- 53 H. Lischka, T. Müller, P. G. Szalay, I. Shavitt, R. M. Pitzer and R. Shepard, *WIREs Comput. Mol. Sci.*, 2011, **1**, 191–199.
- 54 H. Lischka, R. Shepard, R. M. Pitzer, I. Shavitt, M. Dallos, T. Müller, P. G. Szalay, M. Seth, G. S. Kedziora, S. Yabushita and Z. Zhang, *Phys. Chem. Chem. Phys.*, 2001, **3**, 664–673.
- 55 *BAGEL, Brilliantly Advanced General Electronic-structure Library*. <http://www.nubakery.org> under the GNU General Public License.
- 56 T. Shiozaki, *WIREs Comput. Mol. Sci.*, 2018, **8**, e1331.
- 57 Y. Shao, Z. Gan, E. Epifanovsky, A. T. B. Gilbert, M. Wormit, J. Kussmann, A. W. Lange, A. Behn, J. Deng, X. Feng, D. Ghosh, M. Goldey, P. R. Horn, L. D. Jacobson, I. Kaliman, R. Z. Khaliullin, T. Kus, A. Landau, J. Liu, E. I. Proynov, Y. M. Rhee, R. M. Richard, M. A. Rohrdanz, R. P. Steele, E. J. Sundstrom, H. L. Woodcock, III, P. M. Zimmerman, D. Zuev, B. Albrecht, E. Alguire, B. Austin, G. J. O. Beran, Y. A. Bernard, E. Berquist, K. Brandhorst, K. B. Bravaya, S. T. Brown, D. Casanova, C.-M. Chang, Y. Chen, S. H. Chien, K. D. Closser, D. L. Crittenden, M. Diedenhofen, R. A. DiStasio, Jr., H. Do, A. D. Dutoi, R. G. Edgar, S. Fatehi, L. Fusti-Molnar, A. Ghysels, A. Golubeva-Zadorozhnaya, J. Gomes, M. W. D. Hanson-Heine, P. H. P. Harbach, A. W. Hauser, E. G. Hohenstein, Z. C. Holden, T.-C. Jagau, H. Ji, B. Kaduk, K. Khistyayev, J. Kim, J. Kim, R. A. King, P. Klunzinger, D. Kosenkov, T. Kowalczyk, C. M. Krauter, K. U. Lao, A. D. Laurent, K. V. Lawler, S. V. Levchenko, C. Y. Lin, F. Liu, E. Livshits, R. C. Lochan, A. Luenser, P. Manohar, S. F. Manzer, S.-P. Mao, N. Mardirossian, A. V. Marenich, S. A. Maurer,

- N. J. Mayhall, E. Neuscammann, C. M. Oana, R. Olivares-Amaya, D. P. O'Neill, J. A. Parkhill, T. M. Perrine, R. Peverati, A. Prociuk, D. R. Rehn, E. Rosta, N. J. Russ, S. M. Sharada, S. Sharma, D. W. Small, A. Sodt, T. Stein, D. Stueck, Y.-C. Su, A. J. W. Thom, T. Tsuchimochi, V. Vanovschi, L. Vogt, O. Vydrov, T. Wang, M. A. Watson, J. Wenzel, A. White, C. F. Williams, J. Yang, S. Yeganeh, S. R. Yost, Z.-Q. You, I. Y. Zhang, X. Zhang, Y. Zhao, B. R. Brooks, G. K. L. Chan, D. M. Chipman, C. J. Cramer, W. A. Goddard, III, M. S. Gordon, W. J. Hehre, A. Klamt, H. F. Schaefer, III, M. W. Schmidt, C. D. Sherrill, D. G. Truhlar, A. Warshel, X. Xu, A. Aspuru-Guzik, R. Baer, A. T. Bell, N. A. Besley, J.-D. Chai, A. Dreuw, B. D. Dunietz, T. R. Furlani, S. R. Gwaltney, C.-P. Hsu, Y. Jung, J. Kong, D. S. Lambrecht, W. Liang, C. Ochsenfeld, V. A. Rassolov, L. V. Slipchenko, J. E. Subotnik, T. Van Voorhis, J. M. Herbert, A. I. Krylov, P. M. W. Gill and M. Head-Gordon, *Mol. Phys.*, 2015, **113**, 184–215.
- 58 M. Barbatti, M. Ruckebauer, F. Plasser, J. Pittner, G. Granucci, M. Persico and H. Lischka, *WIREs Comput. Mol. Sci.*, 2014, **4**, 26–33.
- 59 M. Barbatti, G. Granucci, M. Ruckebauer, F. Plasser, R. Crespo-Otero, J. Pittner, M. Persico and H. Lischka, *NEWTON-X: A package for Newtonian dynamics close to the crossing seam, version 2*, <http://www.newtonx.org>.
- 60 T. N. Karsili, M. Thodika, L. Nguyen and S. Matsika, *Chemical Physics*, 2018, **515**, 434–440.
- 61 R. Shepard, *Int. J. Quantum Chem.*, 1987, **31**, 33–44.
- 62 R. Shepard, H. Lischka, P. G. Szalay, T. Kovar and M. Ernzerhof, *J. Chem. Phys.*, 1992, **96**, 2085–2098.
- 63 H. Lischka, M. Dallos, P. G. Szalay, D. R. Yarkony and R. Shepard, *J. Chem. Phys.*, 2004, **120**, 7322–7329.
- 64 M. Dallos, H. Lischka, R. Shepard, D. R. Yarkony and P. G. Szalay, *J. Chem. Phys.*, 2004, **120**, 7330–7339.
- 65 B. Vlaisavljevich and T. Shiozaki, *J. Chem. Theory Comput.*, 2016, **12**, 3781–3787.
- 66 J. W. Park and T. Shiozaki, *J. Chem. Theory Comput.*, 2017, **13**, 3676–3683.
- 67 J. W. Park and T. Shiozaki, *J. Chem. Theory Comput.*, 2017, **13**, 2561–2570.
- 68 M. Barbatti, G. Granucci, M. Ruckebauer, F. Plasser, R. Crespo-Otero, J. Pittner, M. Persico and H. Lischka, *NEWTON-X: A package for Newtonian dynamics close to the crossing seam, version 2.2*, <http://www.newtonx.org>.
- 69 L. B. Clark, G. G. Peschel and I. Tinoco, *J. Phys. Chem.*, 1965, **69**, 3615–3618.
- 70 J. C. Tully, *J. Chem. Phys.*, 1990, **93**, 1061–1071.
- 71 G. Granucci and M. Persico, *J. Chem. Phys.*, 2007, **126**, 134114.
- 72 C. Zhu, S. Nangia, A. W. Jasper and D. G. Truhlar, *J. Chem. Phys.*, 2004, **121**, 7658–7670.
- 73 F. Plasser, S. Mai, M. Fumanal, E. Gindensperger, C. Daniel and L. González, *J. Chem. Theory Comput.*, 2019, **15**, 5031–5045.

- 74 P. Chakraborty, Y. Liu, T. Weinacht and S. Matsika, *J. Chem. Phys.*, 2020, **152**, 174302.
- 75 J. Towns, T. Cockerill, M. Dahan, I. Foster, K. Gaither, A. Grimshaw, V. Hazlewood, S. Lathrop, D. Lifka, G. D. Peterson, R. Roskies, J. R. Scott and N. Wilkins-Diehr, *Comput. Sci. Eng.*, 2014, **16**, 62–74.
- 76 S. Mai, M. Richter, M. Heindl, M. F. S. J. Menger, A. Atkins, M. Ruckenbauer, F. Plasser, M. Oppel, P. Marquetand and L. González, *SHARC2.0: Surface Hopping Including Arbitrary Couplings — Program Package for Non-Adiabatic Dynamics*, sharc-md.org, 2018.
- 77 E. Epifanovsky, K. Kowalski, P.-D. Fan, M. Valiev, S. Matsika and A. I. Krylov, *J. Phys. Chem. A*, 2008, **112**, 9983–9992.
- 78 T. Gustavsson, Á. Bányász, E. Lazzarotto, D. Markovitsi, G. Scalmani, M. J. Frisch, V. Barone and R. Improta, *J. Amer. Chem. Soc.*, 2006, **128**, 607–619.
- 79 J. Lorentzon, M. P. Fuelscher and B. O. Roos, *J. Amer. Chem. Soc.*, 1995, **117**, 9265–9273.
- 80 T. Fleig, S. Knecht and C. Hättig, *J. Phys. Chem. A*, 2007, **111**, 5482–5491.
- 81 T. Climent, R. González-Luque, M. Merchán and L. Serrano-Andrés, *Chem. Phys. Lett.*, 2007, **441**, 327 – 331.
- 82 M. Schreiber, M. R. Silva-Junior, S. P. A. Sauer and W. Thiel, *J. Chem. Phys.*, 2008, **128**, 134110.
- 83 L. Buschhaus, J. Rolf and K. Kleineremanns, *Phys. Chem. Chem. Phys.*, 2013, **15**, 18371–18377.
- 84 B. Barc, M. Ryszka, J. Spurrell, M. Dampc, P. Limão-Vieira, R. Parajuli, N. J. Mason and S. Eden, *J. Chem. Phys.*, 2013, **139**, 244311.
- 85 B. K. McFarland, J. P. Farrell, S. Miyabe, F. Tarantelli, A. Aguilar, N. Berrah, C. Bostedt, J. D. Bozek, P. H. Bucksbaum, J. C. Castagna, R. N. Coffee, J. P. Cryan, L. Fang, R. Feifel, K. J. Gaffney, J. M. Glowonia, T. J. Martinez, M. Mucke, B. Murphy, A. Natan, T. Osipov, V. S. Petrović, S. Schorb, T. Schultz, L. S. Spector, M. Swiggers, I. Tenney, S. Wang, J. L. White, W. White and M. Gühr, *Nat. Commun.*, 2014, **5**, 4235.
- 86 T. J. A. Wolf, R. H. Myhre, J. P. Cryan, S. Coriani, R. J. Squibb, A. Battistoni, N. Berrah, C. Bostedt, P. Bucksbaum, G. Coslovich and et al., *Nat. Commun.*, 2017, **8**, 29.
- 87 W. Hua, S. Mukamel and Y. Luo, *J. Phys. Chem. Lett.*, 2019, **10**, 7172–7178.

Table of Contents

High level multi-reference non-adiabatic dynamics simulations reveal that uracil's photoexcited S_2 state decays very fast without any significant trapping.

